Optics Letters

Diamond sodium guide star laser

Xuezong Yang,[1,2,3,*] Ondrej Kitzler,[1] David J. Spence,[1] Zhenxu Bai,[1,3] Yan Feng,[2] and Richard P. Mildren[1]

[1]MQ Photonics Research Centre, Department of Physics and Astronomy, Macquarie University, Sydney, NSW 2109, Australia
[2]Shanghai Institute of Optics and Fine Mechanics, Chinese Academy of Sciences, Jiading, Shanghai 201800, China
[3]Center for Advanced Laser Technology, Hebei University of Technology, Tianjin 300401, China
*Corresponding author: xuezong.yang@hdr.mq.edu.au

Received 10 January 2020; revised 27 February 2020; accepted 27 February 2020; posted 28 February 2020 (Doc. ID 387879); published 20 March 2020

Laser guide stars based on the mesospheric sodium layer are becoming increasingly important for applications that require correction of atmospheric scintillation effects. Despite several laser approaches being investigated to date, there remains great interest in developing lasers with the necessary power and spectral characteristics needed for brighter single or multiple guide stars. Here we propose and demonstrate a novel, to the best of our knowledge, approach based on a diamond Raman laser with intracavity Type I second-harmonic generation pumped using a 1018.4 nm fiber laser. A first demonstration with output power of 22 W at 589 nm was obtained at 18.6% efficiency from the laser diode. The laser operates in a single longitudinal mode (SLM) with a measured linewidth of less than 8.5 MHz. The SLM operation is a result of the strong mode competition arising from the combination of a spatial-hole-burning-free gain mechanism in the diamond and the role of sum frequency mixing in the harmonic crystal. Continuous tuning through the Na D line resonance is achieved by cavity length control, and broader tuning is obtained via the tuning of the pump wavelength. We show that the concept is well suited to achieve much higher power and for temporal formats of interest for advanced concepts such as time-gating and Larmor frequency enhancement. © 2020 Optical Society of America

https://doi.org/10.1364/OL.387879

Wavefront distortions induced by atmospheric turbulence obstruct the full-resolution imaging of large ground-based optical telescopes. Adaptive optical systems [1] are used to sense and compensate for these aberrations in real time. Artificial sodium laser guide stars (LGSs) generated by 589 nm laser induced fluorescence of sodium atoms in the mesosphere are considered to be a critical component for state-of-the-art systems for aberration correction [2,3]. Such systems are also of intense interest for applications in optical free-space communications [4], space debris tracking [5], sodium layer lidar [6–8], and mesospheric magnetometry [9–11]. The photon return intensity of the sodium beacon is a key factor in determining the quality of image correction. Though early systems used a laser linewidth that matched the Na Doppler broadened width of the D_2 ($3^2S_{1/2} - 3^2P_{3/2}$) line (~1 GHz [12]), higher photon returns are obtained by using laser linewidths less than the natural linewidth (~8 MHz) tuned to the high oscillator strength D_{2a} $F = 2$ to $F = 3$, hyperfine transition at 589.15908 nm [13]. Additional schemes for enhancing photon return include "repumping," circular polarization, Larmor frequency pulses, and polarization switching [12–15]. A combination of these techniques, along with a high average power beam (e.g., ~100 W/m^2 sodium saturation intensity [13]), is expected to significantly boost the LGS brightness. A pulsed illumination of the 10 km thick sodium layer for microsecond durations, coupled with time-gated imaging, is also proposed to mitigate Rayleigh scattering noise, star elongation, and the fratricide problem for multiple guidestar systems [14].

The specific combination of wavelength, linewidth, diffraction-limited beam quality, and average power (>10 W) for sodium guide star lasers is a notorious challenge. Though the earliest systems were dye lasers [16–18], most systems now are based on sum-frequency-generation (SFG) of solid-state lasers [19–24] and Yb-fiber pumped Raman fiber lasers [25–27]. Two prominent examples include a continuous-wave (cw) 50 W SFG laser deployed at the Starfire Optical Range 3.5 m telescope [19] and a 22 W cw Raman fiber at the Very Large Telescope UT4 [25]. Optically pumped semiconductor lasers are also being investigated with the reported maximum output power up to 12 W [28,29].

Raman lasers based on diamond are an interesting candidate for high-power yellow lasers owing to a high-gain Raman mode at 39.9 THz [30], which provides a convenient way to generate the 1178 nm fundamental laser from the Yb gain band and outstanding potential for high average power [31–34]. Though the gain bandwidth of the diamond Raman medium is at least 45 GHz, the lasers favor single longitudinal mode operation (SLM) without the use of wavelength selective cavity elements or ring cavities due to the absence of spatial hole burning in the Raman gain medium [35–37]. Intracavity harmonic generation provides an additional mechanism for mode competition [38], as well as efficient wavelength conversion to the visible using Type I phase-matching schemes. This approach has recently led to a demonstration of 38 W of a quasi-cw SLM laser at 620 nm [39]. Therefore, with an appropriate choice of pump

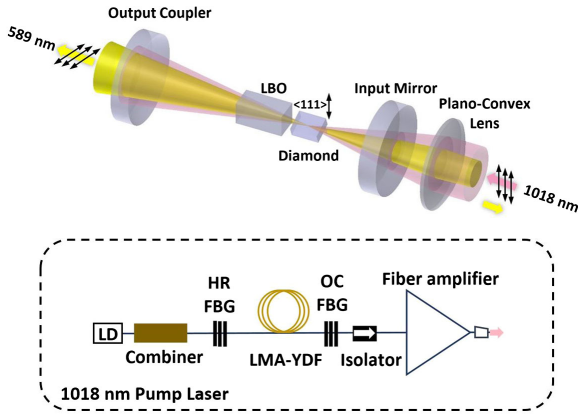

Fig. 1. Top, schematic of the 589 nm diamond Raman laser with intracavity SHG. Bottom, the 1018 nm pump laser. HR FBG, highly reflective fiber Bragg grating; OC FBG, output coupling fiber Bragg grating; LMA-YDF, large-mode-area Yb^{3+}-doped fiber; LD, laser diode.

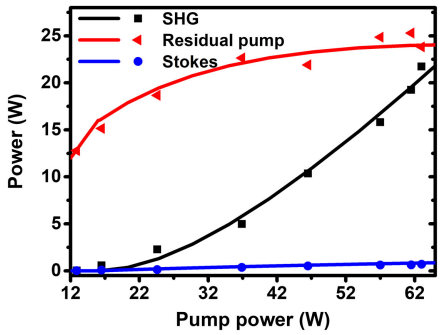

Fig. 2. Measured powers of SHG (black square), residual pump (red triangle), and Stokes (blue circle), and model calculated powers of SHG (black solid), residual pump (red solid) and Stokes (blue solid) as a function of incident pump power.

wavelength, there are promising practical strategies for achieving a high-power and narrow-linewidth laser tuned to the Na resonance.

In this Letter, we report a cw diamond Raman laser with SLM output tuned to the Na D_2 lines. With a 63 W 1018 nm Yb pump laser, we have achieved a highly efficient 589 nm laser with output power above 20 W. We show that the scheme is well suited to meet the needs of future LGSs tuned to Na hyperfine levels in either continuous- or microsecond-pulsed formats.

The experimental configuration, shown in Fig. 1, was adapted from Ref. [39]. Cavity mirror coatings and intracavity elements were selected to minimize losses at the pump and Stokes wavelengths. The cavity is composed of a 50 mm radius of curvature input mirror highly transmitting (98.0%T) at 1018 nm and highly reflective (99.9%R) at 1178 nm, and an output coupler highly reflective (99.98%R) at the pump and Stokes wavelengths. The pump was focused into the diamond crystal (8 mm × 4 mm × 1.2 mm) with a waist radius of 27 μm using a plano-convex $f = 50$ mm lens. The second-harmonic generation (SHG) crystal was LiB_3O_5 (LBO) cut at $\theta = 90°$, $\phi = 0°$ with dimensions of 10 mm × 4 mm × 4 mm, and heated to the phase-matching temperature of 41°C. The direction of pump polarization, diamond <111> axis, and LBO slow axis were aligned parallel to each other, providing the highest Raman gain [40] and SHG angle match. The coatings of the input mirror and output coupler were partially transmissive at 589 nm, 35% and 39% respectively, resulting in double-ended output beams. The Stokes spectrum was monitored using a VIPA spectrometer (HF-8997-2, LightMachinery; resolution of 0.8 GHz at 1178 nm) which was capable of resolving individual modes (laser cavity free-spectral range [FSR] 0.9 GHz).

The 1018 nm Yb-doped fiber (YDF) pump laser experimental setup shown in the dashed box at the bottom of the Fig. 1 was constructed including an oscillator with a pair of fiber Bragg gratings (FBGs) at 1018 nm and one stage of a YDF amplifier. A large-mode-area active fiber was used to suppress amplified spontaneous emission at around 1030 nm [41]. An oscillator power of 1.2 W was amplified to 75 W at the diode power of 118 W. Due to the thermal sensitivity of the FBGs, the wavelength was tunable over 90 GHz by varying the temperature of the FBGs from 10°C to 40°C.

After collimation, feedback-isolation, beam expansion, and focusing, the pump beam was inserted into the diamond Raman and second-harmonic generation (SHG) resonator. Owing to a high-Q cavity with extremely low round-trip cavity loss and output coupling at Stokes wavelength, the threshold of the Stokes-resonator was as low as 13 W. At an injection pump power of 63 W, the double-ended SHG powers increased up to a maximum of 22 W with a leakage Stokes power of only 0.7 W.

The optical-to-optical conversion efficiency from 1018 to 589 nm was 34.9%, a marked improvement compared to the 11.8% from 1064 to 620 nm reported in Ref. [39]. The higher conversion efficiency in this case is attributed to the combination of low cavity loss and tight pump focusing. The overall conversion efficiency from the amplifier diode pump power at 976 to 589 nm was 18.6%, which is a record for any diode-pumped LGS system, to the best of our knowledge. The measured powers of SHG (black square), residual pump (red triangle), and Stokes (blue circle) as a function of incident pump power are plotted in Fig. 2, along with the model curves for the system using the analytical approach for the intracavity SHG Raman laser detailed in Ref. [42]. The model is based on a double-pass pumped resonator with intracavity SHG, assuming that all beams are Gaussian, and thermal effects are neglected. In the calculation, the total round-trip cavity loss at Stokes wavelength was 0.92%, including crystal absorption, scattering, and surface reflection. The output coupling at the Stokes wavelength was 0.12%, the diamond Raman gain was 10 cm/GW, the Stokes beam waist was 32 μm, and the beam diameter in LBO was 180 μm. The model results agree well with the experimental data indicating that the power budget for the system is well understood.

By tuning the pump wavelength, the output wavelength was tunable from 588.97 to 589.19 nm (190 GHz), as shown in Fig. 3(a). Output coinciding with the sodium D_{2a} line at 589.16 nm was obtained at the temperature of 37°C. The laser was a SLM over the investigated ranges of power and wavelength. For a fixed pump wavelength, continuous mode-hop-free tuning over a small fraction (~7%) of the Raman linewidth was achieved by varying the cavity length. Using a piezoelectric translation stage on the output coupler, tuning over 3.7 GHz was demonstrated for a cavity change of 2.3 μm

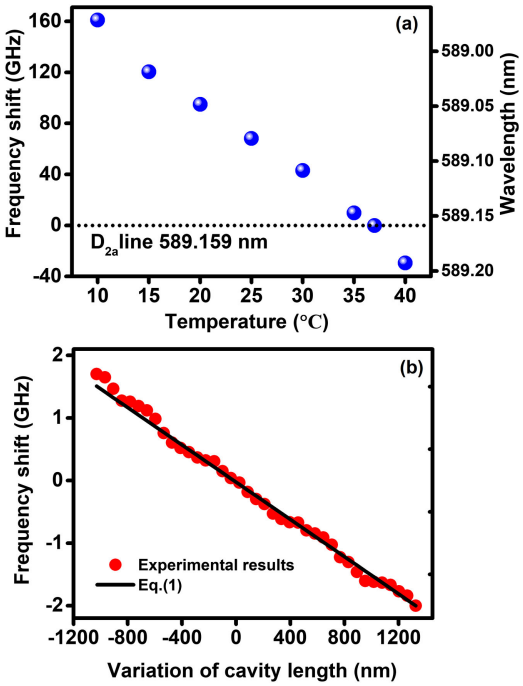

Fig. 3. Frequency shift as a function of (a) FBG temperature and (b) cavity length.

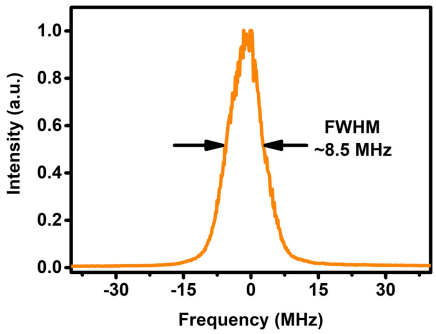

Fig. 4. Scanning Fabry–Perot interferometer trace of the single-frequency 589 nm laser.

[Fig. 3(b)]. This range exceeds the 1.71 GHz interval between the main D_{2a} line and the D_{2b} "repumping" line, as well as the 3 GHz D_2 Doppler broadened linewidth. We note some slight departure of the output frequency from the calculated frequency shift $\Delta\nu$ as a function of cavity length ΔL:

$$\Delta\nu = c/\lambda\left[1-(1\pm\Delta L/L)^{1/2}\right], \quad (1)$$

where c is the speed of light, λ is the Stokes wavelength, and L is the optical length of the cavity, which we attribute to small thermal drifts in cavity length over the 2 min period of measurement.

The output spectrum was measured using a scanning F-P interferometer (SA200-5B, ThorLabs) FSR of 1.5 GHz. The output had an instrument-limited linewidth of 8.5 MHz full-width at half-maximum, as shown in Fig. 4.

Due to the LMA active fiber (core diameter of 20 μm) in the 1018 nm laser, some higher-order transverse modes were excited providing an output beam quality of $M^2 = 1.23$ at the maximum output power. Due to diamond's capacity for extremely rapid heat dissipation [32] and the tendency for the Raman gain to excite the fundamental transverse mode [43], a near-diffraction-limited beam was obtained for the full power range ($M^2 = 1.08$ at 22 W).

The output polarization was linear with a polarization-extinction ratio of 18 dB and orthogonal to the polarization of the incident pump.

The power, frequency, linewidth, and diffraction-limited output beam already meet the basic requirements for a sodium LGS. We expect that the system is also well suited to power scaling to a much higher level by using higher-power 1018 nm pumps such as those reported in [44–46]. The main obstacles for power scaling are thermal lensing in the diamond (due to Raman phonon excitation and impurity absorption) and in the LBO (impurity absorption only). For the diamond, thermal lensing is strongly mitigated due to its high thermal conductivity and low thermal expansion coefficient such that no major lensing is expected at power levels below 100 W [47]. Based on the analysis for the 620 nm laser of Ref. [42], it is found that a thermal lens in the LBO is an important factor depending on the impurity level. A power level of approximately 100 W was predicted for a standard level of impurity absorption $\alpha = 0.1\%/\text{cm}$ and higher using lower absorption LBO. We note that intracavity lasers involving LBO have been demonstrated at continuous powers up to 1.5 kW [48]; hence, powers in excess of 100 W are likely to be possible without major design changes.

In addition to power scaling, the laser system is also promising for enhancing the LGS signal-to-noise through temporal and frequency modulations. Our concept may be readily adapted to generate microsecond duration-pulsed output to enable time-gated systems and Larmor frequency enhancement. In this case, the necessary high average power 1018 nm microsecond-pulsed pump laser may be realized by modulating pump diodes in the YDF amplifier [27] or the seed laser [49]. Furthermore, the tunability of output frequency via cavity length provides a method to chirp the output frequency to compensate for the recoil of sodium atoms that result after photon absorption and emission [50]. The recommended chirp rate (~0.5 MHz/μs [50]) may be readily achieved using conventional piezo elements.

In summary, a 22 W cw 589 nm laser with near-diffraction-limited beam quality generated in a standing-wave diamond Raman resonator with intracavity SHG is demonstrated for the first time, to the best of our knowledge. The pump was a 1018 nm YDF laser composed of a FBG oscillator and one stage of YDF amplifier. A 34.9% conversion efficiency from the pump to yellow and an 18.6% conversion efficiency from diode to yellow were achieved. The spatial-hole-burning-free Raman gain and additional gain competition provided by harmonic mixing mediated the SLM operation at the Stokes and SHG. The measured linewidth of SLM output at 589 nm was less than 8.5 MHz. By tuning the pump wavelength, output from 588.97 to 589.19 nm was demonstrated. Mode-hop-free tuning across the Doppler broadened width of 3 GHz was achieved by scanning the cavity length.

Funding. Australian Research Council (DP150102054, LP160101039); Air Force Office of Scientific Research (FA2386-18-1-4117).

Acknowledgment. The authors of this Letter are grateful for the joint degree program (Cotutelle) between Macquarie University and the Shanghai Institute of Optics and Fine Mechanics, Chinese Academy of Sciences.

Disclosures. The authors declare no conflicts of interest.

REFERENCES

1. H. W. Babcock, Publ. Astron. Soc. Pac. **65**, 229 (1953).
2. C. E. Max, S. S. Olivier, H. W. Friedman, J. An, K. Avicola, B. V. Beeman, H. D. Bissinger, J. M. Brase, G. V. Erbert, D. T. Gavel, K. Kanz, M. C. Liu, B. Macintosh, K. P. Neeb, J. Patience, and K. E. Waltjen, Science **277**, 1649 (1997).
3. C. S. Gardner, B. M. Welsh, and L. A. Thompson, Proc. IEEE **78**, 1721 (1990).
4. R. Mata-Calvo, D. B. Calia, R. Barrios, M. Centrone, D. Giggenbach, G. Lombardi, P. Becker, and I. Zayer, Proc. SPIE **10096**, 100960R (2017).
5. C. D'Orgeville, F. Bennet, M. Blundell, R. Brister, A. Chan, M. Dawson, Y. Gao, N. Paulin, I. Price, F. Rigaut, I. Ritchie, M. Sellars, C. Smith, K. Uhlendorf, and Y. Wang, Proc. SPIE **9148**, 91483E (2014).
6. T. Li, X. Fang, W. Liu, S.-Y. Gu, and X. Dou, Appl. Opt. **51**, 5401 (2012).
7. C. S. Gardner, Proc. IEEE **77**, 408 (1989).
8. T. D. Kawahara, S. Nozawa, N. Saito, T. Kawabata, T. T. Tsuda, and S. Wada, Opt. Express **25**, A491 (2017).
9. J. M. Higbie, S. M. Rochester, B. Patton, R. Holzlöhner, D. Bonaccini Calia, and D. Budker, Proc. Natl. Acad. Sci. USA **108**, 3522 (2011).
10. T. Fan, X. Yang, J. Dong, L. Zhang, S. Cui, J. Qian, R. Dong, K. Deng, T. Zhou, K. Wei, Y. Feng, and W. Chen, J. Geophys. Res. **124**, 7505 (2019).
11. F. Pedreros Bustos, D. Bonaccini Calia, D. Budker, M. Centrone, J. Hellemeier, P. Hickson, R. Holzlöhner, and S. Rochester, Nat. Commun. **9**, 3981 (2018).
12. B. M. Welsh and C. S. Gardner, Appl. Opt. **28**, 4141 (1989).
13. P. D. Hillman, J. D. Drummond, C. A. Denman, and R. Q. Fugate, Proc. SPIE **7015**, 70150L (2008).
14. R. Rampy, D. Gavel, S. M. Rochester, and R. Holzlöhner, J. Opt. Soc. Am. B **32**, 2425 (2015).
15. T. Fan, T. Zhou, and Y. Feng, Sci. Rep. **6**, 19859 (2016).
16. L. A. Thompson and C. S. Gardner, Nature **328**, 229 (1987).
17. I. L. Bass, R. E. Bonanno, R. P. Hackel, and P. R. Hammond, Appl. Opt. **31**, 6993 (1992).
18. S. Rabien, R. I. Davies, T. Ott, J. Li, S. Hippler, and U. Neumann, Proc. SPIE **4839**, 393 (2003).
19. C. A. Denman, J. D. Drummond, M. L. Eickhoff, R. Q. Fugate, P. D. Hillman, S. J. Novotny, and J. M. Telle, Proc. SPIE **6272**, 62721L (2006).
20. I. Lee, N. Vanasse, Z. Prezkuta, K. Groff, J. Roush, N. Rogers, E. Andrews, G. Moule, B. Tiemann, A. K. Hankla, S. M. Adkins, and C. d'Orgeville, Proc. SPIE **7015**, 70150N (2008).
21. Y. Hayano, S. Oya, M. Hattori, Y. Saito, M. Watanabe, O. Guyon, Y. Minowa, S. E. Egner, M. Ito, V. Garrel, S. Colley, and T. Golota, Proc. SPIE **7736**, 77360N (2010).
22. J. Dawson, A. Drobshoff, R. Beach, M. Messerly, S. Payne, A. Brown, D. Pennington, D. Bamford, S. Sharpe, and D. Cook, Proc. SPIE **6102**, 61021F (2006).
23. Y. Lu, L. Zhang, X. Xu, H. Ren, X. Chen, X. Wei, B. Wei, Y. Liao, J. Gu, F. Liu, L. Xu, J. Wang, T. Chen, M. Wan, W. Zhang, C. Tang, and G. Fan, Opt. Express **27**, 20282 (2019).
24. K. Jin, K. Wei, L. Feng, Y. Bo, J. Zuo, M. Li, H. Fu, X. Dai, Q. Bian, J. Yao, C. Xu, Z. Wang, Q. Peng, X. Xue, X. Cheng, C. Rao, Z. Xu, and Y. Zhang, Publ. Astron. Soc. Pac. **127**, 749 (2015).
25. M. Enderlein and W. G. Kaenders, Opt. Photonik **11**, 31 (2016).
26. M. Enderlein, A. Friedenauer, R. Schwerdt, P. Rehme, D. Wei, V. Karpov, B. Ernstberger, P. Leisching, W. R. L. Clements, and W. G. Kaenders, Proc. SPIE **9148**, 914807 (2014).
27. L. Zhang, H. Jiang, S. Cui, J. Hu, and Y. Feng, Laser Photonics Rev. **8**, 889 (2014).
28. C. d'Orgeville, G. J. Fetzer, S. Floyd, L. Hill, S. Rako, N. Woody, S. Sandalphon, F. Bennet, A. Bouchez, Y. Gao, M. Goodwin, A. Lambert, J. Mason, F. Rigaut, S. Ryder, D. Shaddock, and R. Sharp, Proc. SPIE **10703**, 107030T (2018).
29. E. Kantola, T. Leinonen, S. Ranta, M. Tavast, and M. Guina, Opt. Express **22**, 6372 (2014).
30. A. D. Greentree and S. Prawer, Nat. Photonics **4**, 202 (2010).
31. R. J. Williams, J. Nold, M. Strecker, O. Kitzler, A. McKay, T. Schreiber, and R. P. Mildren, Laser Photonics Rev. **9**, 405 (2015).
32. Z. Bai, R. J. Williams, H. Jasbeer, S. Sarang, O. Kitzler, A. McKay, and R. P. Mildren, Opt. Lett. **43**, 563 (2018).
33. R. J. Williams, O. Kitzler, Z. Bai, S. Sarang, H. Jasbeer, A. McKay, S. Antipov, A. Sabella, O. Lux, D. J. Spence, and R. P. Mildren, IEEE J. Sel. Top. Quantum Electron. **24**, 1 (2018).
34. H. Zhang, P. Li, and X. Chen, Appl. Opt. **56**, 6973 (2017).
35. O. Lux, S. Sarang, O. Kitzler, D. J. Spence, and R. P. Mildren, Optica **3**, 876 (2016).
36. O. Kitzler, J. Lin, H. M. Pask, R. P. Mildren, S. C. Webster, N. Hempler, G. P. A. Malcolm, and D. J. Spence, Opt. Lett. **42**, 1229 (2017).
37. Q. Sheng, R. Li, A. J. Lee, D. J. Spence, and H. M. Pask, Opt. Express **27**, 8540 (2019).
38. K. I. Martin, W. A. Clarkson, and D. C. Hanna, Opt. Lett. **22**, 375 (1997).
39. X. Yang, O. Kitzler, D. J. Spence, R. J. Williams, Z. Bai, S. Sarang, L. Zhang, Y. Feng, and R. P. Mildren, Opt. Lett. **44**, 839 (2019).
40. A. Sabella, J. A. Piper, and R. P. Mildren, Opt. Lett. **35**, 3874 (2010).
41. Y. Midilli, O. B. Efunbajo, B. Şimşek, and B. Ortaç, Appl. Opt. **56**, 7225 (2017).
42. H. Jasbeer, R. J. Williams, O. Kitzler, A. McKay, and R. P. Mildren, Opt. Express **26**, 1930 (2018).
43. J. T. Murray, W. L. Austin, and R. C. Powell, Opt. Mater. **11**, 353 (1999).
44. Y. Glick, Y. Sintov, R. Zuitlin, S. Pearl, Y. Shamir, R. Feldman, Z. Horvitz, and N. Shafir, J. Opt. Soc. Am. B **33**, 1392 (2016).
45. M. Jiang, P. Zhou, H. Xiao, and P. Ma, High Power Laser Sci. Eng. **3**, e25 (2015).
46. P. Yan, X. Wang, D. Li, Y. Huang, J. Sun, Q. Xiao, and M. Gong, Opt. Lett. **42**, 1193 (2017).
47. S. Antipov, A. Sabella, R. J. Williams, O. Kitzler, D. J. Spence, and R. P. Mildren, Opt. Lett. **44**, 2506 (2019).
48. C. Stolzenburg, W. Schüle, V. Angrick, M. Bouzid, and A. Killi, Proc. SPIE **8959**, 89590O (2014).
49. X. Yang, L. Zhang, S. Cui, T. Fan, J. Dong, and Y. Feng, Opt. Lett. **42**, 4351 (2017).
50. E. Kibblewhite, in *Advanced Maui Optical and Space Surveillance Technologies Conference* (2009).